ARTICLE

Hydrangea-like NiCo-based Bimetal-organic Frameworks, and their Pros and Cons as Supercapacitor Electrode Materials in Aqueous Electrolytes

Qiaoqin Li,[a] Xiaoqin Wang,*[a,b] Nana Yang,[a] Fan He,[a] Yufei Yang,[a] Bohua Wu,[a] Jia Chu,[a] Anning Zhou,[a,b] and Shanxin Xiong*[a,b]

Abstract. Hydrangea-like NiCo-based bimetal-organic frameworks (NiCo-MOF) are synthesized in DMF-EtOH solution via a solvo-thermal method, using 4,4′-biphenyldicarboxylic acid as a ligand. NiCo-MOF having a highest capacity of 1056.6 F·g^{-1} at 0.5 A·g^{-1} and 457.7 F·g^{-1} even at 10 A·g^{-1} is achieved at a Ni/Co/BPDC molar ratio of 1:1:1, a temperature of 170 °C and a reaction time of 12 hours. It exhibits secondary 3D microsphere structures assembled by primary 2D nanosheet structures, good crystalline structure and good thermal stability below 350 °C in air. All the electrochemical data show that NiCo-MOF has the pros and cons as supercapacitor electrode materials in aqueous electrolytes. On the one hand, NiCo-MOF has a high capacity even at a high current density, low internal resistance, charge-

transfer resistance and ion diffusion impendence, owing to the ordered coordination structure, 2D nanosheet structure and 3D assembled microsphere structure of NiCo-MOF. On the other hand, the cycling stability and rate capability are not ideal enough due to the hydrolysis of coordination bonds in aqueous electrolytes, especially, in alkaline solution. The good dispersion and high electrochemical activity of metal ions bring a high capacity for NiCo-MOF, but they result in the poor stability of NiCo-MOF. In the future work, finding a suitable organic electrolyte is an effective way to enhance the cycling stability of NiCo-MOF as well as deriving more stable skeleton materials from NiCo-MOF.

Introduction

Supercapacitors are a high-capacity energy storage device bridging the gap between electrolytic capacitors and rechargeable batteries. They can store 10 to 100 times more energy per unit volume or mass than electrolytic capacitors, can reserve and deliver charge much faster than batteries, and can tolerate many more charge and discharge cycles than rechargeable batteries. They are greatly applied in the fields requiring many rapid charge/discharge cycles rather than long term compact energy storage. At present, they have been used for regenerative braking, short-term energy storage or burst-mode power delivery within cars, buses, trains, cranes and elevators.[1] Supercapacitor performances are mainly determined by electrode materials. The general electrode materials are carbon materials, metal oxides/hydroxides and conductive polymers. Among them, carbon materials have a large surface area, good conductivity, strong chemical stability, but a low specific capacitance and low energy density. Metal oxides/hydroxides own a large specific capacitance, high energy density, but a

poor conductivity and narrow potential window. Conductive polymers possess a large specific capacitance and low cost, but they are easily detached due to the expansion in the charge and discharge process.[2]

Metal organic frameworks (MOFs) are a new member of the porous material family and have been greatly attracted due to its adjustable pore size, large specific surface area and abundant organic functional groups, having potential applications in supercapacitors,[3–6] lithium-ion batteries, catalysts, sensors, medicine and so on. Many studies have demonstrated that medium strength MOFs can be readily obtained using poly-carboxylic acids as monodentate, bidentate or multidentate ligands. Some reports[7–13] confirm that BPDC can coordinate with monometallic Co, Ni, Cd, Zn, Ba, Zr, or bimetallic Zn(Co, Ni, Cd) to construct porous mononuclear, dinuclear, or multinuclear MOFs with different dimensionalities. Furthermore, 4,4′-biphenyldicarboxylic acid (BPDC) owns more flexible and larger conjugated structure than 1,4-benzenedicarboxylic acid (BDC) due to the biphenyl group, which possibly results in higher conductivity, larger pore size and more variable structure for MOFs.

Ni-based MOFs usually possess high capacitance and irregular shapes[4,7] whereas Co-based MOFs always own regular and stable morphologies and low capacitance.[14] Considered that both nickel ions and cobalt ions have a divalent state, adjacent atomic number and very close ionic radius, it is possible that nickel ions and cobalt ions simultaneously coordinate with a ligand to construct bimetallic MOFs crystals presenting a little lattice distortion. Moreover, some reports have confirmed that two different metal ions may coordinate with a

* Dr. X. Wang
  Fax: +86-29-85583183
  E-Mail: wangxq@xust.edu.cn
* Dr. S. Xiong
  E-Mail: xiongsx@xust.edu.cn
[a] College of Chemistry & Chemical Engineering
  Xi'an University of Science & Technology
  Xi'an, 710054, P. R. China
[b] Key Laboratory of Coal Resources Exploration and Comprehensive Utilization, MLR.
  Xi'an, 710021, P. R. China
  ⌨ Supporting information for this article is available on the WWW under **http://dx.doi.org/10.1002/zaac.201900035** or from the author.

ligand to form a homogeneous bimetallic MOFs rather than a mixture of two monometallic MOFs, and synthesizing bimetallic MOFs is becoming a new strategy for enhancing framework stability and properties.[15–19] At present, only a few NiCo-based MOFs have been reported as electrode materials presenting high electrochemical activity and energy storage capacity, in which terephthalic acid-pyrazine,[16] 2-methylimidazole,[17] 1,3,5-benzenetricarboxylic acid,[18] and benzenedicarboxylic acid (BDC)[19] are used as ligands.

Herein, a series of hydrangea-like NiCo-MOFs are synthesized via a simple solvothermal approach, depending coordination reactions between metal ions and BPDC in a DMF-EtOH solution. Their morphologies, microstructures, pore structure, thermal stability and capacitance performances are evaluated by SEM, TEM, XRD, FTIR, Raman, physical adsorption and desorption, TG and electrochemical measurements, respectively. As expected, the hydrangea-like NiCo-MOF has a large capacitance, low internal resistance, charge-transfer resistance, and ion diffusion impendence. The pros and cons are described in detail about NiCo-MOF as supercapacitor electrode materials in aqueous electrolytes, and the corresponding essential reasons are discussed, and the modified approaches in the future work are offered.

Results and Discussion

Morphologies and Capacitance Performances of NiCo-MOF Synthesized under Various Reaction Conditions

In order to investigate the optimal Ni/Co/BPDC molar ratio, reaction temperature and time, a series of NiCo-MOFs are synthesized under various conditions. Their morphologies are observed by SEM measurements and their electrochemical behaviors are performed by CV and GCD tests. SEM images are shown in Figure 1, and CV and GCD curves are exhibited in Figure 2. It can be seen from Figure 1 that all the NiCo-MOFs exhibit secondary 3D hydrangea-like microsphere structures assembled by primary 2D nanosheet structures. In Figure 1a–c, NiCo-MOF microspheres at Ni/Co/BPDC molar ratio of 1:1:1 have better dispersion, more uniform size, better sphericity and integrity than 1:1:2 and 1:2:2. According to the single crystal analysis of Co-MOF using BPDC as a ligand via a hydrothermal approach in literature,[13] the molar ratio is determined to 1 between metal ions and BPDC in the Co-MOF single crystals. The ratio of 1:1:2 is just right, but the corresponding NiCo-MOF microspheres present the most serious agglomeration and non-uniform size, and some of them are defective. Whereas, the other two NiCo-MOF microspheres exhibit the better dispersion and sphere integrity due to the excess (metal ions/BPBC) molar ratio. It indicates that excess metal ions in the reaction system are favorable for forming well-dispersed and complete NiCo-MOF microspheres. By the weighing and calculating, the yields of NiCo-MOF at various ratios of 1:1:1, 1:1:2, and 1:2:2 are 1.05 g·g^{-1} (BPDC), 0.82 g·g^{-1} (BPDC), and 0.91 g·g^{-1} (BPDC), respectively. Moreover, CV and GCD curves in Figure 2a and b show that NiCo-MOF at the ratio of 1:1:1 has a much larger CV circle

area and more discharge time than the other two, indicating that it has a largest specific capacitance among the three. Furthermore, a pair of redox peaks of the 1:1:1 sample in Figure 2a corresponds a couple of quite reversible redox reactions, indicating that NiCo-MOF electrode has an excellent faradic pseudocapacitance. Hence, it is better to adjust the Ni/Co/BPDC molar ratio to 1:1:1.
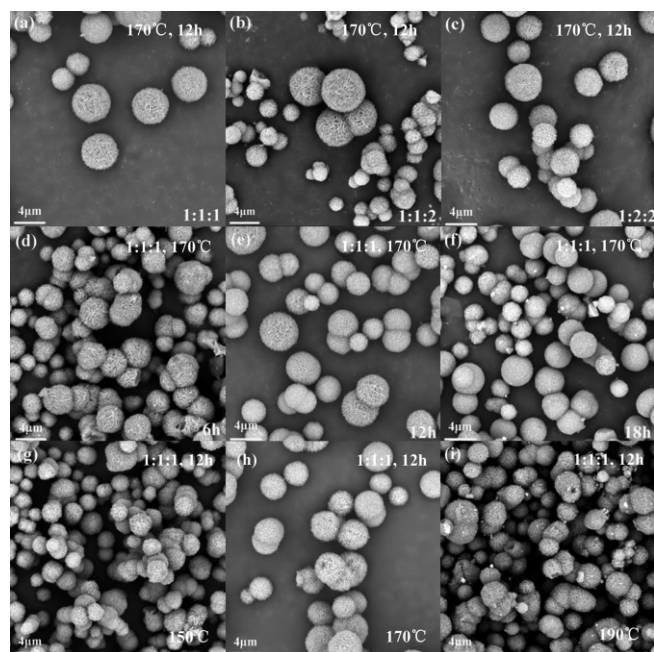
Figure 1. SEM images of bimetallic NiCo-MOF particles synthesized under various reaction conditions.

In Figure 1d–f, NiCo-MOF microspheres synthesized in 12 h exhibit the best dispersion, most uniform size, best sphericity, and integrity among the three. In Figure 2c–d, NiCo-MOF synthesized in 12 h presents a much larger CV circle area and more discharge time than 6 h and 18 h. Moreover, the yields of NiCo-MOF synthesized in diverse reaction time of 6 h, 12 h, and 18 h are calculated to 1.01 g·g^{-1} (BPDC), 1.05 g·g^{-1} (BPDC), and 0.94 g·g^{-1} (BPDC), respectively. Therefore, controlling the reaction time to 12 h can facilitate uniform, well-dispersed and complete microspheres.

In Figure 1g–i, NiCo-MOF microspheres synthesized at 170 °C have better dispersion, more uniform size, better sphericity, and integrity than the other two. In Figure 2e–f, NiCo-MOF microspheres synthesized at 170 °C possess a largest CV circle area and most discharge time among the three. Additionally, the yields of NiCo-MOF synthesized at different temperature of 150, 170, and 190 °C are 1.06 g·g^{-1} (BPDC), 1.05 g·g^{-1} (BPDC), and 1.05 g·g^{-1} (BPDC), respectively. Thus, the temperature of 170 °C is regarded as an optimal condition.

In Figure 1, it is also found that NiCo-MOF microspheres have looser surface at conditions of lower (metal ions/BPBC) molar ratio, less reaction time, and lower temperature. NiCo-MOF microspheres containing more slit-shaped micro-mesopores can be assembled by adjusting the reaction conditions, which are favorable for the immigration and storage of electrolytic ions. Through the comparison of SEM tests and electro-
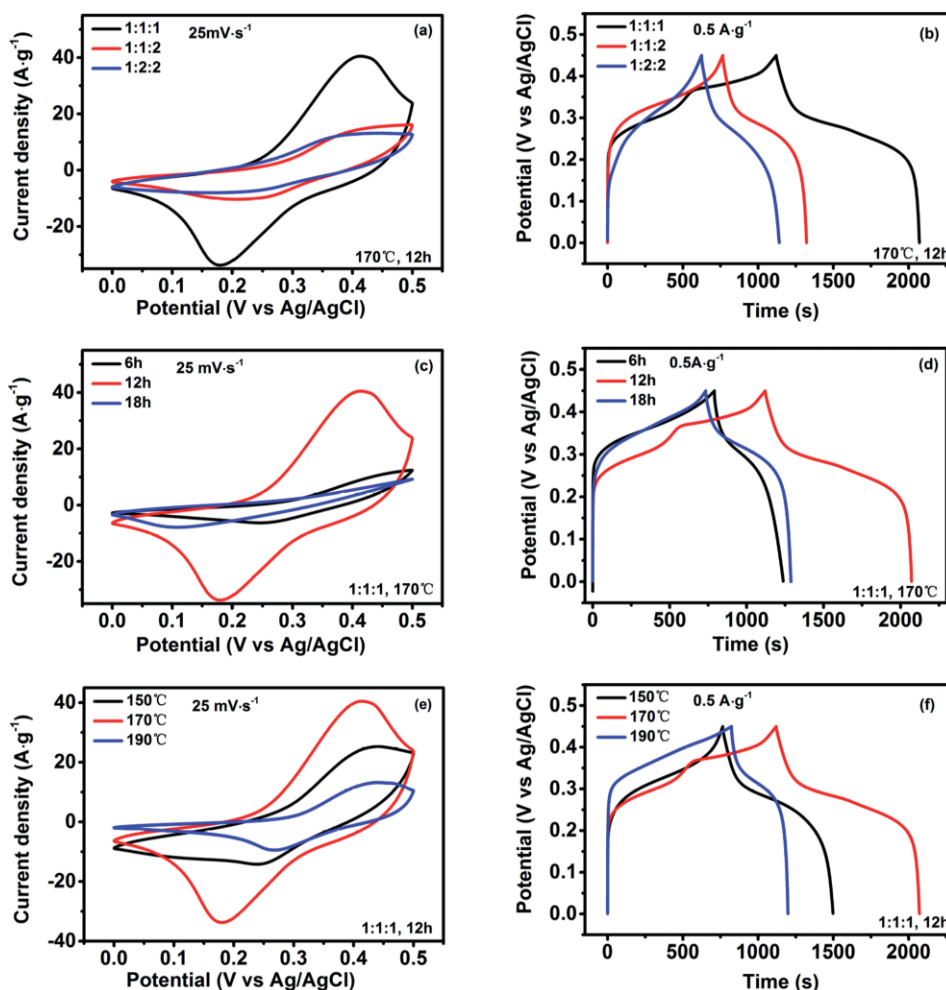
Figure 2. Electrochemical behaviors of bimetallic NiCo-MOF electrodes synthesized under various reaction conditions.

chemical measurements, it can be determined that the optimal process is a Ni/Co/BPDC molar ratio of 1:1:1, temperature of 170 °C and reaction time of 12 h for synthesizing NiCo-MOF with a highest capacity. In this paper, unless otherwise stated, NiCo-MOF is designated as a sample synthesized in this optimal process.

Figure 3 shows the elemental mapping of C, O, Ni, and Co in one NiCo-MOF microsphere. The distributions of four elements are similar to the morphology of NiCo-MOF microsphere and they are homogeneously distributed throughout the whole microsphere. Moreover, the C and O distribution are denser than the Co and Ni distribution. All these demonstrate that each NiCo-MOF microsphere is a compound composed of nickel ions, cobalt ions and BPDC ligands. The metal content in the optimal NiCo-MOF are determined by an ICP test of the digested and diluted NiCo-MOF solution. The nickel and cobalt mass content are 13.53 wt% and 16.55 wt%, respectively. The Ni/Co atomic ratio is about 1/1.21, which indicates that cobalt ions have stronger coordination ability than nickel ions.
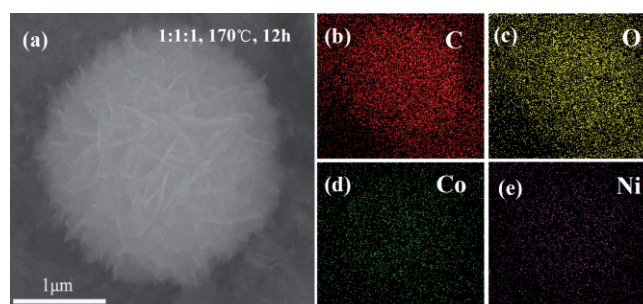
Figure 3. SEM image (a) and the corresponding C (b), O (c), Co (d), and Ni (e) elemental mapping of optimal NiCo-MOF particles.

Morphologies, Microstructures, and Capacitance Performances of Monometallic Ni(Co)-MOF and Bimetallic NiCo-MOF

For the comparison with bimetallic NiCo-MOF, monometallic Ni-MOF and Co-MOF are also synthesized at 170 °C for 12 h. Through the weighing and calculating, the yields of NiCo-MOF, Ni-MOF and Co-MOF are 1.05 g·g⁻¹ (BPDC),

0.86 g·g⁻¹ (BPDC), and 0.79 g·g⁻¹ (BPDC), respectively. The morphologies of three MOFs are investigated by SEM tests and shown in Figure 4. All the three MOFs also demonstrate secondary 3D microsphere structures assembled by primary 2D nanosheet structures. Among them, the particle size and surface porosity of NiCo-MOF microspheres are between Ni-MOF and Co-MOF. Meanwhile, NiCo-MOF microspheres have better sphericity and dispersion than the other two. As shown in Figure 4a and b, Ni-MOF microspheres are assembled by the smallest 2D nanosheets and present the smallest sphere-like shapes, but they are seriously aggregated. In Figure 4c and d, Co-MOF microspheres are assembled by the biggest 2D nanosheets and present the biggest flower-like shapes. They have a good dispersion, loose surface but a poor sphericity. In Figure 4e and f, NiCo-MOF microspheres exhibit hydrangea-like shapes, and demonstrate better sphericity than Co-MOF and better dispersibility than Ni-MOF. In order to further study how NiCo-MOF hydrangeas are assembled, TEM tests are conducted to analyze their internal structures. TEM images in Figure 4g and h exhibit that there are many voids in each NiCo-MOF hydrangea, which stem from the loose assembly of primary nanosheets. These voids may become the storage space of electrolyte ions. TEM tests further confirm that the as-synthesized NiCo-MOF hydrangeas are assembled by 2D nanosheets and many voids exist in their internal structures.
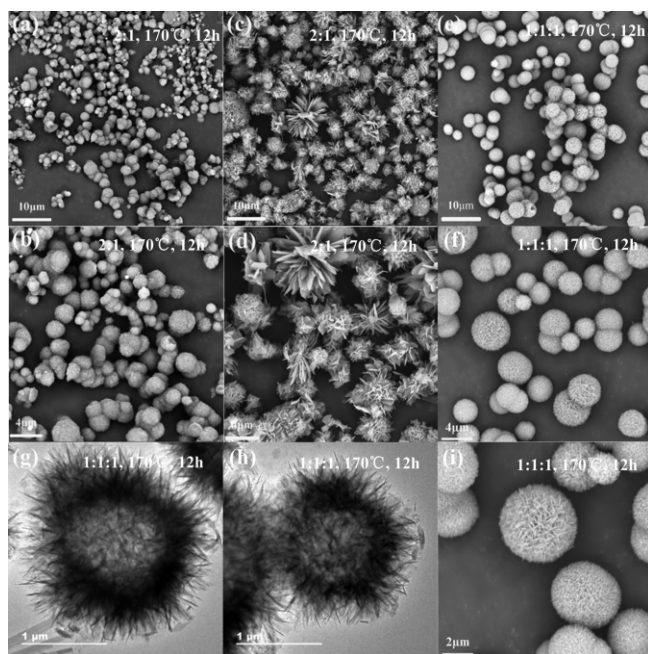
Figure 4. SEM images of Ni-MOF (a) (b), Co-MOF (c) (d), optimal NiCo-MOF (e) (f) (i) particles at a Ni/Co/BPDC molar ratio of 1:1:1, a temperature of 170 °C and a reaction time of 12 h and TEM images of optimal NiCo-MOF particles (g) (h).

The crystalline structures of three MOFs are further analyzed by the XRD tests. The XRD patterns in Figure 5a show that all the three MOFs have a group of similar sharp diffraction peaks at 2θ values of 6.1°, 12.4°, 15.4°, 19.7°, 29.4° and 40.8°, assigned to NiCo-MOF crystals using BPDC as a ligand because all the peak sites are well consistent with that of the reported NiCo-MOF[2] and Co-MOF[20] using BPDC as a ligand via a hydrothermal method, other than the relative peak strength. The results indicate that three samples have crystalline structures of MOFs indeed, and their crystalline structures are similar and their crystallinity is good. The chemical structures of three MOFs are also investigated by FTIR and Raman measurements. The FTIR spectra in Figure 5b show that three MOFs have similar infrared absorption peaks, indicating they consist of the same organic units. A group of peaks at 1596, 825, 761, and 679 cm⁻¹ are assigned to the characteristic mode of aromatic ring.[21] The two strong bands at 1541 and 1381 cm⁻¹ are ascribed to the asymmetric and symmetric stretching modes of the coordinated carboxyl group from BPDC.[7–22] All these confirm that BPDC ligands exist in the as-synthesized NiCo-MOF. Moreover, two bands at 441 cm⁻¹ and 528 cm⁻¹ are associated with Ni–O and Co–O stretching vibrations, indicating that metal ions have coordinated with BPDC.

The Raman spectra of three MOFs are exhibited in Figure 5c. The four Raman bands at 1583, 1428, 1285, and 1143 cm⁻¹ are attributed to C–H in-plane bending mode of aromatic ring, and the two bands at 855 cm⁻¹ and 3067 cm⁻¹ correspond to C–H out-of-plane bending mode of aromatic ring. Additionally, a couple of bands at 413 cm⁻¹ and 627 cm⁻¹ are assigned to the Ni–O and Co–O stretching vibration. All the Raman bands well coincide with that of the reported NiCo-MOF synthesized via a hydrothermal approach.[23] These Raman results are also in good agreement with the above FTIR analysis.

Meanwhile, the electrochemical behaviors of Ni-MOF, Co-MOF, and NiCo-MOF are evaluated by CV, GCD, and EIS tests, and the results are shown in Figure 6. Compared with Ni-MOF and Co-MOF, NiCo-MOF demonstrates the larger circle area in CV curves of Figure 6a and the longer discharge time in GCD curves of Figure 6b, indicating that bimetallic NiCo-MOF has a higher charge storage capability than monometallic Ni-MOF or Co-MOF. This conclusion can be affirmed by the calculation results from GCD curves at 0.5 A·g⁻¹, in which the specific capacitance of NiCo-MOF is 1056.6 F·g⁻¹, larger than that of Ni-MOF (708.8 F·g⁻¹) and Co-MOF (153.0 F·g⁻¹). Furthermore, the rate capability of three MOFs in Figure 6c exhibits that NiCo-MOF has a higher specific capacitance than Ni-MOF and Co-MOF at any current density ranging from 0.5 A·g⁻¹ to 10 A·g⁻¹, which further confirms the above conclusion.

EIS tests can get a further insight about the origin of three MOFs' electrochemical performances. The original Nyquist plots of Ni-MOF, Co-MOF, and NiCo-MOF are drawn in Figure 6d. The magnified plots at low frequency part and the suitable equivalent circuit for Nyquist plots are also exhibited in the inset. Three plots are composed of a depressed semicircle at high frequency part, the slope of the 45° portion at medium frequency part and a straight line at low frequency part. The depressed semicircle is related to charge-transfer impedance (R_{ct}) at the electrode/electrolyte interface. The intercept of Z' axis is associated with the internal resistance (R_s) of active
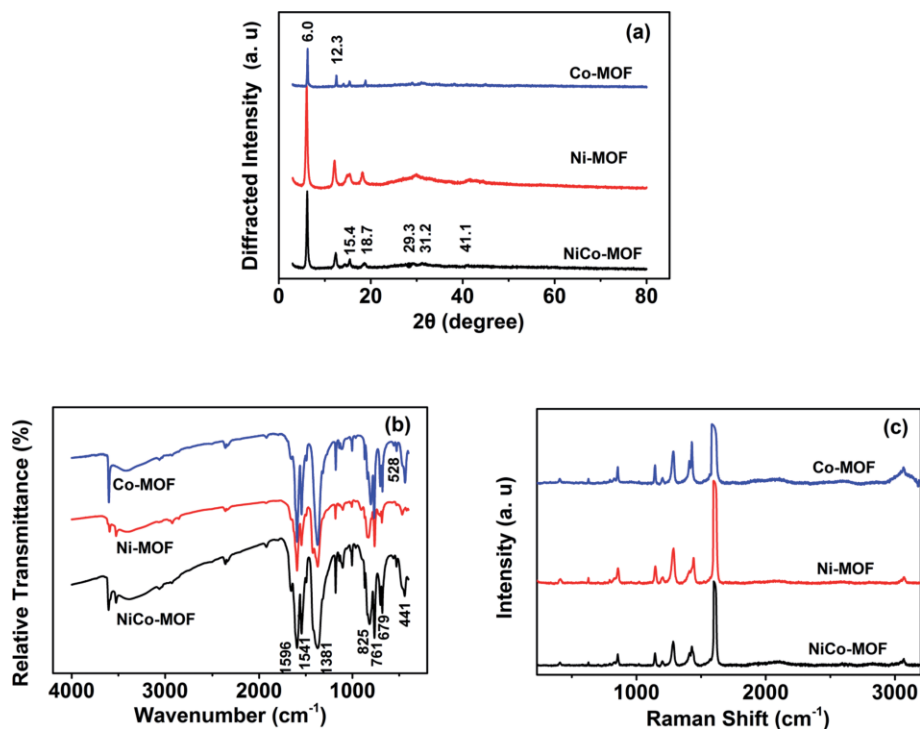
Figure 5. XRD patterns (a), FTIR spectra (b) and Raman spectra (c) of Ni-MOF, Co-MOF and optimal NiCo-MOF particles.
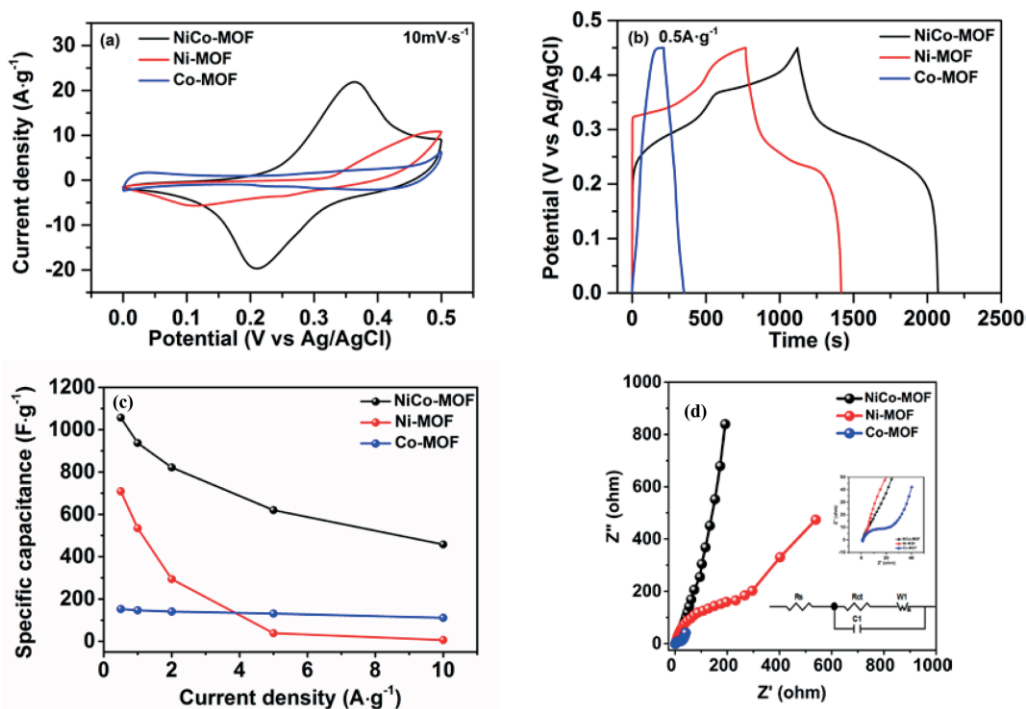
Figure 6. CV curves (a), GCD curves (b), rate capability curve (c), Nyquist plots (d) of Ni-MOF, Co-MOF and optimal NiCo-MOF electrodes.

electrodes. The slope of straight line at low frequency part is in connection with the impendence of ion diffusion inside the electrode.[24] The Nyquist plot of NiCo-MOF shows a very steeper line than Ni-MOF and Co-MOF at low frequency region and its vertical angle is close to 90°, indicating the fast ion migration in electrode materials due to a low ion diffusion

impendence and a high capacity as observed in Figure 6a and b. Fitted by equivalent circuit, NiCo-MOF presents the lower charge-transfer resistance R_{ct} (0.1 Ω) than Ni-MOF (0.4 Ω) and Co-MOF (53.7 Ω), indicating that NiCo-MOF more easily deliver charges at the electrode/electrolyte interface than Ni-MOF and Co-MOF. Additionally, the internal resistance R_s of

NiCo-MOF, Ni-MOF, and Co-MOF are 2.0 Ω, 2.2 Ω, and 2.8 Ω, respectively, suggesting that three MOFs electrodes have a good conductivity. The EIS results indicate that bimetallic NiCo-MOF has a lower internal resistance, charge-transfer resistance and ion diffusion impendence than monometallic Ni-MOF or Co-MOF, which are the essential reasons why bimetallic NiCo-MOF possesses a higher capacity than monometallic MOFs.

Pore Structure, Thermal Stability, and other Capacitance Performances of Optimal NiCo-MOF

The pore structure of optimal NiCo-MOF is analyzed on an adsorption analyzer, and the N_2 adsorption-desorption isotherm and pore distribution curve are exhibited in Figure 7. The isotherm presents an obvious hysteresis loop, which is usually located in the multilayer range of physisorption isotherms and generally associated with capillary condensation in mesopore structures. This hysteresis loop meets the Type H3, whose adsorption branch of the isotherm is like a combination of the Types I and II isotherm. The front part in the P/P_0 range of 0 and 0.5 is attributed to monolayer adsorption. The latter part in the P/P_0 range of 0.5 and 1 is related to multilayer adsorption, capillary condensation and even liquid condensation. The isotherm does not exhibit any limiting adsorption at high P/P_0, which is often observed with aggregates of plate-like particles giving rise to slit-shaped pores.[25] From Figure 1, Figure 3, and Figure 4, a plenty of slit-shaped pores are obviously produced in the NiCo-MOF microspheres through the assembly of NiCo-MOF nanosheets. The pore distribution curve in Figure 7b demonstrates that the slit-shaped mesopores with diameters of 3–15 nm make the greatest contribution to the pore volume, especially 3.5–5 nm. Calculated from the N_2 adsorption data, the BET surface area and average pore width of NiCo-MOF are 44.1 $m^2 \cdot g^{-1}$ and 15.1 nm, respectively. All these confirm that most slit-shaped pores are mesoporous in NiCo-MOF microspheres, which are favorable for the intercalation of electrolyte ions. In addition, the low surface area is associated with the unconnected slit-shaped pores. As observed in Figure 4g–h, a high density ring exists between porous interior and loose surface, attributed to the tight assembly of NiCo-MOF nanosheets.

The thermal stability of NiCo-MOF is evaluated by thermogravimetric (TG) analysis in air atmosphere. The corresponding TG and derivative thermogravimetric (DTG) curves are drawn in Figure 8. Five mass losses can be found. Three small losses of ca. 9 % at the temperature range of 25–350 °C are attributed to the removal of the adsorbed water and carbon oxides, and a few coordinated DMF. Two large losses of 56 % at the range of 350–800 °C derive from the collapse and decomposition of organic skeleton, especially, the exclusion of CO_2 from the evolution of carboxylic groups. The overall mass loss of NiCo-MOF is about 64.16 % and the final products are metal oxides. The mass is almost unchanged at 450–800 °C, indicating that the formation reaction of metal oxides has been terminated at 450 °C. Based on the TG/DTG analysis, it can be concluded that the as-synthesized NiCo-MOF is stable below 350 °C in air, which is more stable than NiCo-MOF synthesized via a hydrothermal method.[2]
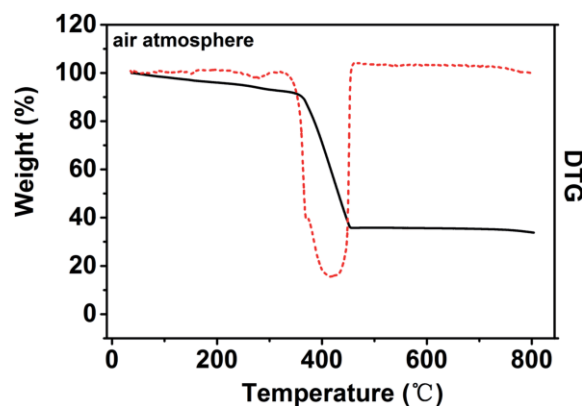
Figure 8. TG and DTG curves of optimal NiCo-MOF particles in air atmosphere.

CV tests at various scan rates and GCD tests at different current densities are further evaluated the electrochemical behaviors of NiCo-MOF. All the CV curves in Figure 9a present a pair of strong redox peaks at ca. 0.35 V/0.20 V corresponding to M(III)↔M(IV), intimating a pseudocapacitive behavior. Moreover, as the scan rate increases, the oxidation peak shifts a more positive position and the reduction peak shifts a more negative position, deriving from an increasing polarization at a higher scan rate. Some GCD curves in Figure 9b exhibit two couples of GCD redox plateaus at ca. 0.35 V/0.25 V and ca. 0.25 V/0.20 V, assigned to M(III)↔M(IV) and M(II)↔M(III), respectively. The pseudocapacitive feature of NiCo-MOF is
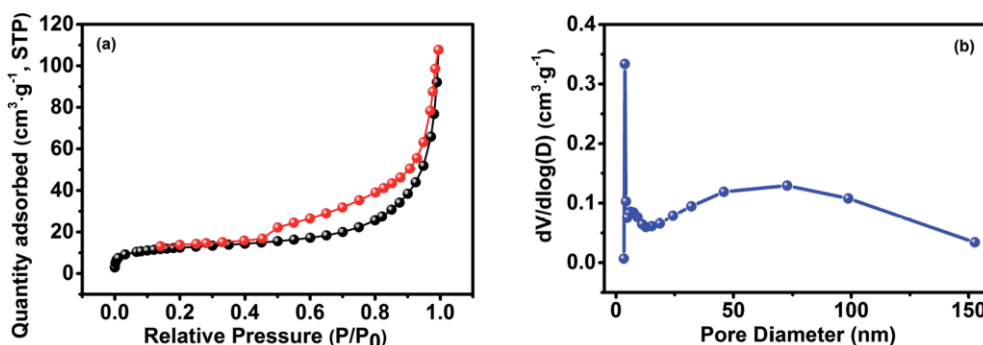
Figure 7. N_2 adsorption-desorption isotherm (a) and pore distribution (b) of optimal NiCo-MOF particles.
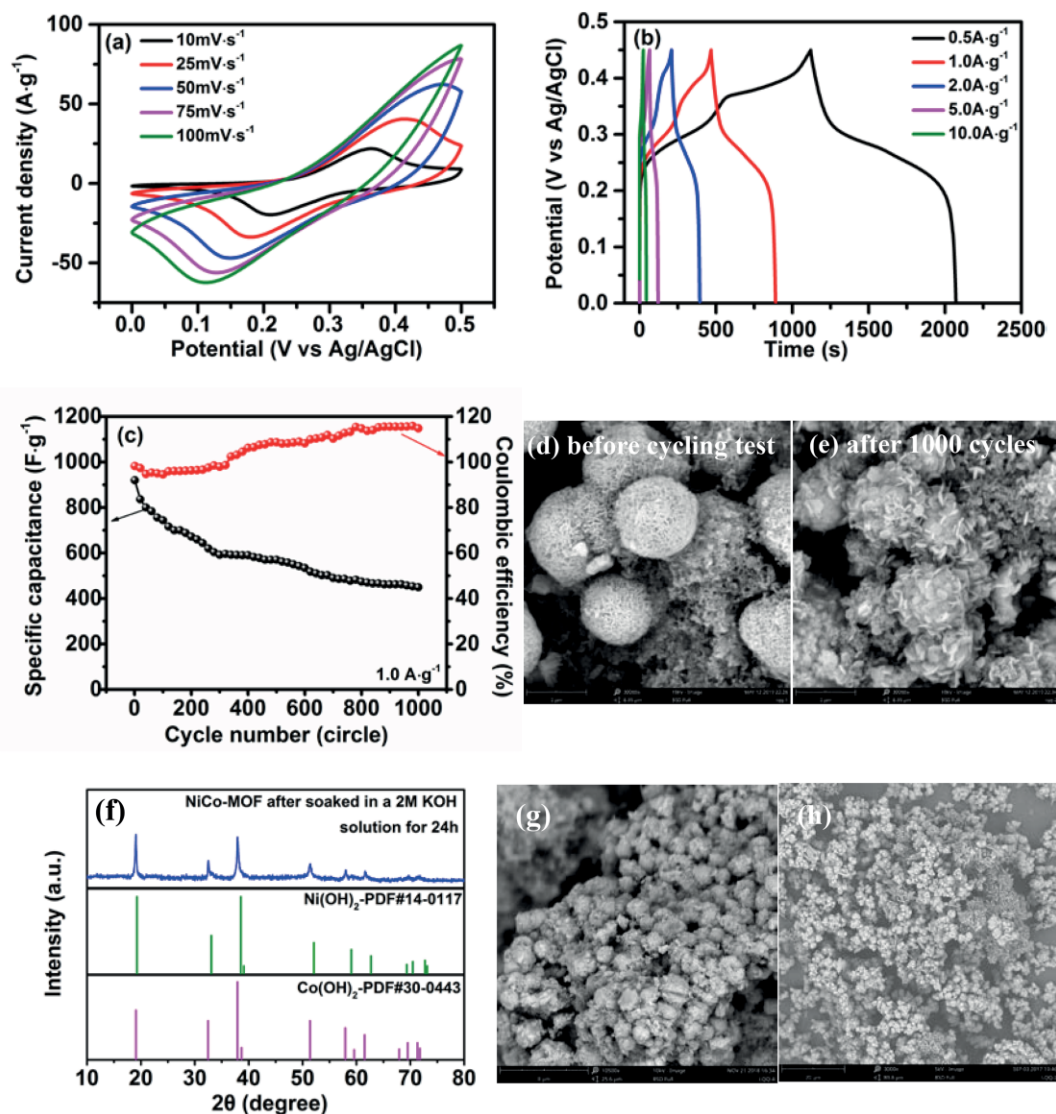
Figure 9. CV curves at different scan rates (a), GCD curves at various current densities (b), cycling stability and coulombic efficiency at 1 A/g (c) of optimal NiCo-MOF electrodes in a three-electrode system; SEM images (d) (e) of optimal NiCo-MOF electrodes using graphite paper as current collector before and after 1000-cycle GCD tests; XRD image (f) and SEM pattern (g) of optimal NiCo-MOF after soaked in a 2 M KOH solution for 24 h, and SEM image (h) NiCo-MOF after soaked in deionized water for 50 d.

further affirmed, well coinciding with the CV results. Another couple of CV redox peaks related with M(III)$\leftrightarrow M$(IV) do not occur in CV curves, originating that this redox reaction is too fast to record. Calculated from GCD curves, specific capacitances of NiCo-MOF are 1056.6 F·g^{-1} (0.5 A·g^{-1}), 936.8 F·g^{-1} (1 A·g^{-1}), 821.3 F·g^{-1} (2 A·g^{-1}), 620.0 F·g^{-1} (5 A·g^{-1}), and 457.7 F·g^{-1} (10 A·g^{-1}), respectively. The change of specific capacitance with current density can be seen visually in Figure 6c, demonstrating that NiCo-MOF still maintains a high capacity of 457.7 F·g^{-1} even at 10 A·g^{-1} although the rate capability of NiCo-MOF is not ideal enough. The cycling stability is one of the most important factors for electrode materials in practical applications. The cycling stability of NiCo-MOF is examined by GCD measurements at 1 A·g^{-1} for 1000 cycles and the results are displayed in Figure 9c. The specific capacitance of NiCo-MOF at 1 A·g^{-1} drops gradually to

481.1 F·g^{-1} from the initial value of 920.0 F·g^{-1} during 700 cycles and tends to be stable over 700 cycles. It eventually reaches 449.2 F·g^{-1} (48.8 % of initial value) after 1000 cycles. The coulombic efficiency of NiCo-MOF decreases slightly first and then gradually increases from the initial value of 98.2 % to 114.9 % after 1000 cycles. Why is the cycling capacitance of NiCo-MOF not stable enough in aqueous electrolyte? The SEM images of NiCo-MOF electrodes using graphite paper as current collector are observed before and after 1000 GCD cycles and showed in Figure 9d and e. The morphologies of NiCo-MOF microspheres have no change in the electrode fabrication process. However, the morphologies of microsphere-like active materials after 1000 GCD cycles have some changes, which are assembled by many regular hexagonal nanosheets and have a looser surface than the tightly assembled NiCo-MOF microspheres. But they remain the micro-

sphere-shaped morphologies of NiCo-MOF assembled by nanosheets. Furthermore, the XRD and SEM test of NiCo-MOF particles after soaked in a 2 M KOH solution for 24 h are conducted and the results are shown in Figure 9f and g, respectively. The SEM image demonstrates that some nanosheets on the NiCo-MOF microsphere surface are peeled off or reconstructed after the soaking. The serious aggregation of microspheres originates that the soaked sample is not ground. The XRD pattern exhibits that most NiCo-MOF on microsphere surface is converted to $Ni(OH)_2$ and $Co(OH)_2$ because no NiCo-MOF peaks are found. Thus, the regular hexagonal nanosheets on the microsphere surface in Figure 9e can be deduced to be $Ni(OH)_2$ and $Co(OH)_2$. $Ni(OH)_2$ and $Co(OH)_2$ are regarded as metal hydroxides possessing high pseudocapacitance.[20,26] Hence, the NiCo-MOF derivatives have been produced in the cycling process and they present a lower capacity than NiCo-MOF. It mainly originates that the electrochemical activity of nickel ions or cobalt ions in NiCo-MOF is much higher than $Ni(OH)_2$ or $Co(OH)_2$, attributed to the particular ordered coordination structure of NiCo-MOF. The SEM image of NiCo-MOF after soaked in deionized water for 50 days is also observed and showed in Figure 9h, which depicts that the morphology of NiCo-MOF have been changed and some NiCo-MOF microspheres are also reconstructed and gathered after the 50-day soaking. It further indicates that NiCo-MOF is not stable in aqueous electrolyte, owing to the hydrolysis of coordination bonds, especially, in alkaline solution.

All the electrochemical data show that NiCo-MOF has the pros and cons as supercapacitor electrode materials in aqueous electrolytes. The optimal NiCo-MOF possesses a high capacity even at high current density, low internal resistance, charge-transfer resistance and ion diffusion impendence as electrode materials in aqueous electrolyte, owing to the ordered coordination structure, 2D nanosheet structure and 3D assembled microsphere structure of NiCo-MOF. The particular structures make metal ions highly dispersed in NiCo-MOF microspheres and entitle NiCo-MOF high electrochemical activity. However, the cycling stability and rate capability are not ideal enough due to the hydrolysis of coordination bonds in aqueous electrolytes. In a word, the high electrochemical activity of NiCo-MOF can bring a large capacitance, but it results in a poor stability. If NiCo-MOF is expected to be stable, its activity has to be sacrificed. In the future work, finding a suitable organic electrolyte may be an effective way to enhance the cycling stability of NiCo-MOF as well as deriving more stable skeleton materials from NiCo-MOF.

Conclusions

A series of hydrangea-like NiCo-MOF are successfully synthesized via a solvothermal method and the optimal process has been discussed. NiCo-MOF presents secondary 3D microsphere structures assembled by primary 2D nanosheet structures, good crystalline structure and good thermal stability below 350 °C in air. Compared with monometallic Ni-MOF and Ni-MOF, bimetallic NiCo-MOF has a lower internal resistance, lower charge-transfer resistance, lower ion diffusion im-

pendence and higher capacity. It exhibits a large specific capacitance of 1056.6 F·g^{-1} at 0.5 A·g^{-1} and 457.7 F·g^{-1} even at 10 A·g^{-1}, and capacitance retention of 449.2 F·g^{-1} at 1 A·g^{-1} after 1000 cycles. All the electrochemical data show that NiCo-MOF has the pro of high capacity and the con of poor cycling stability as supercapacitor electrode materials in aqueous electrolytes. The essential reasons on the pros and cons of capacitance performances of NiCo-MOF in aqueous electrolytes are revealed and the corresponding modified approaches in the future work are suggested.

Experimental Section

Materials: 4,4′-Biphenyldicarboxylic acid was purchased from Aladdin Industrial Corporation, China. $Ni(NO_3)_2 \cdot 6H_2O$, $Co(NO_3)_2 \cdot 6H_2O$, KOH, DMF, EtOH were purchased from local reagent suppliers and used without further purification. Solef 5130-PVDF particles were purchased from Solvay Co., France. Super-P conductive carbon black (Super-P) particles were purchased from Timcal Graphite Co., Switzerland. Nickel foams with a thickness of 1 mm and a density of 300 g·m^{-3} were purchased from Tianjin Aiweixin Chemical Technology Co., China.

Synthesis of NiCo-MOF via a Solvothermal Approach: First, BPDC (0.125 mmol) was dissolved in 22 mL DMF-EtOH solution with a DMF/EtOH volume ratio of 10/1 whilst stirring at 40 °C. Next, $Ni(NO_3)_2 \cdot 6H_2O$ (0.125 mmol) and equimolar $Co(NO_3)_2 \cdot 6H_2O$ were added into the above solution and dissolved whilst stirring at 40 °C. Then, the mixture was promptly transferred into a 45 mL Teflon lined stainless-steel autoclave and heated for 12 h at 170 °C. After the natural cooling, the precipitate was washed several times with DMF and EtOH in turn. Finally, the brown NiCo-MOF particles were achieved with a Ni/Co/BPDC molar ratio of 1:1:1 after dried at 60 °C for 12 h in vacuo.

For comparison, the brown NiCo-MOF particles with different Ni/Co/BPDC molar ratios of 1:1:2 and 1:2:2 were also synthesized according to the above process. Therein, The BPDC concentration was invariable for synthesizing three NiCo-MOF particles. Moreover, the light pink Co-MOF and the light green Ni-MOF particles with a Ni(Co)/BPDC molar ratio of 2:1 were also synthesized according to the above process, in which 0.25 mmol $Co(NO_3)_2 \cdot 6H_2O$ or $Ni(NO_3)_2 \cdot 6H_2O$ were individually added. Furthermore, the brown NiCo-MOF particles with a Ni/Co/BPDC molar ratio of 1:1:1 were prepared in a similar process to the above at various temperature (150 °C, 190 °C) and time (6 h, 18 h).

Measurements: The morphologies of samples were observed on a Phenom/Pro scanning electron microscope, a FEI INSPECT F50 field emission scanning electron microscope and a JEOL JEM-2100 transmission electron microscope, respectively. The contents of nickel and cobalt element in NiCo-MOF were determined by a Varian 715-ES inductively coupled plasma optical emission spectrometer. The crystalline structures were analyzed with a Rigaku Mini Flex 600 diffractometer. The FTIR spectra were recorded with a Thermo Fisher Scientific Nicolet IZ10. The Raman spectra were collected with a Renishaw InVia Raman spectrometer with 532 nm laser source at ambient temperature. The specific surface area and pore structure were analyzed on a Micromeritics ASAP 2020 automatic physical and chemical adsorption analyzer in nitrogen at –196.201 °C as an adsorbent. The thermogravimetric (TG) analysis was performed on a Germany DSC 200PC & TG209C thermogravimetric/differential thermal analyzer

from room temperature to 800 °C at a heating rate of 10 °C·min⁻¹ in air atmosphere.

The electrochemical measurements were conducted in a 2 M KOH electrolyte solution, using an Autolab PGSTAT 302N electrochemical workstation in a three electrode system. An Ag/AgCl electrode with saturated potassium chloride electrolyte was selected as the reference electrode. A platinum plate was used as the counter electrode. The working electrodes were fabricated according to the reported method.[2] The NiCo-MOF active materials were mixed with Super-P particles and then dispersed in DMF for obtaining a suspension liquid. PVDF particles were dissolved in DMF for preparing an adhesive solution. A mixed pasty electrode material was achieved after the PVDF adhesive solution was added into the suspension liquid under agitation. Then the pasty electrode materials were coated evenly on nickel foams with the coating area of 1×1 cm². Last an active electrode was obtained after dried to constant weight in vacuo at 60 °C. Therein, the mass ratio of (active materials)/Super-P/PVDF was controlled to 80/10/10 and the DMF dosage was set to 2 mL·g⁻¹ (active materials). The areal loading mass of active materials on nickel foams was controlled at about 1 mg·cm⁻². CV measurements were carried out between 0 V and 0.5 V at various scan rates. GCD tests were performed from 0 V to 0.4 V at different current densities. The corresponding specific capacitances of active electrodes were calculated from GCD curves according to the equation in literature.[22] EIS measurements were conducted in a frequency range from 100 kHz to 0.01 Hz under open circuit voltage.

Supporting Information (see footnote on the first page of this article): The Supporting Information details the preparation of the samples in Figure 9.

Acknowledgements

References

[1] F. Béguin, E. Raymundo-Piñeiro, E. Frackowiak, *CRC Press.* **2009**, 329–376.

[2] X. Q. Wang, Q. Q. Li, N. N. Yang, Y. F. Yang, F. He, J. Chu, M. Gong, B. H. Wu, R. L. Zhang, S. X. Xiong, *J. Solid State Chem.* **2019**, *270*, 370–378.

[3] Y. H. Wang, B. Bredenkotter, B. Riegera, D. Volkmer, *Dalton Trans.* **2007**, *48*, 689–696.

[4] J. Yang, P. X. Xiong, C. Zheng, H. Y. Qiu, M. D. Wei, *J. Mater. Chem. A* **2014**, *2*, 16640–16644.

[5] Y. Yue, H. Arman, Z. J. Tonzetich, B. Chen, *Z. Anorg. Allg. Chem.* **2019**, *645*, 797–800.

[6] J. Wang, S. Huang, S. Yang, Y. Chen, Y. Wu, N. Li, X. Dong, F. Li, *Z. Anorg. Allg. Chem.* **2019**, *645*, 706–711.

[7] C. Qu, Y. Jiao, B. Zhao, D. C. Chen, R. Q. Zou, K. Walton, M. L. Liu, *Nano Energy* **2016**, *26*, 66–73.

[8] X. R. Hao, G. S. Yang, K. Z. Shao, Z. M. Su, G. Yuan, X. L. Wang, *J. Solid State Chem.* **2013**, *198*, 143–148.

[9] C. Wang, Z. G. Xie, K. E. deKrafft, W. B. Lin, *J. Am. Chem. Soc.* **2011**, *133*, 13445–13454.

[10] Z. Z. Shi, Z. R. Pan, L. Qin, J. L. Zhou, H. J. Zheng, *Cryst. Growth Des.* **2017**, *17*, 2757–2766.

[11] Y. B. Huang, T. F. Liu, J. X. Lin, J. Lü, Z. J. Lin, R. Cao, *Inorg. Chem.* **2011**, *50*, 2191–2198.

[12] T. Yuen, C. L. Lin, J. A. Zan, L. Pan, J. Li, *J. Appl. Phys.* **2005**, *97*, 10B315–3.

[13] L. Pan, N. Ching, X. Y. Huang, J. Li, *Inorg. Chem.* **2000**, *39*, 5333–5340.

[14] R. Díaz, M. G. Orcajo, J. A. Botas, G. Calleja, J. Palma, *Mater. Lett.* **2012**, *68*, 126–128.

[15] X. K. Song, M. Oh, M. S. Lah, *Inorg. Chem.* **2013**, *52*, 10869–10876.

[16] H. Gholipourranjbar, M. Soleimani, H. R. Naderi, *New J. Chem.* **2016**, *40*, 9187–9193.

[17] H. C. Xia, J. A. Zhang, Z. Yang, S. Y. Guo, S. H. Guo, Q. Xu, *Nano-Micro Lett.* **2017**, *4*, 62–72.

[18] S. W. Gao, Y. W. Sui, F. X. Wei, J. Q. Qi, Q. K. Meng, Y. J. Ren, Y. Z. He, *J. Colloid Interface Sci.* **2018**, *531*, 83–90.

[19] S. L. Zhao, Y. Wang, J. C. Dong, C. T. He, H. J. Yin, P. F. An, K. Zhao, X. F. Zhang, C. Gao, L. J. Zhang, J. W. Lv, J. X. Wang, J. Q. Zhang, A. M. Khattak, N. A. Khan, Z. X. Wei, J. Zhang, S. Q. Liu, H. J. Zhao, Z. Y. Tang, *Nature Energy* **2016**, *1*, 16184.

[20] Z. F. Wang, Y. S. Liu, C. W. Gao, H. Jiang, J. M. Zhang, *J. Mater. Chem. A* **2015**, *3*, 20658–20663.

[21] X. D. Guo, L. Y. Wang, S. Yue, D. Y. Wang, Y. L. Lu, Y. F. Song, J. He, *Inorg. Chem.* **2014**, *53*, 12841–12847.

[22] Y. Z. Wang, Y. X. Liu, H. Q. Wang, W. Liu, Y. Li, J. F. Zhang, H. Hou, J. L. Yang, *ACS Appl. Energy Mater.* **2019**, *2*, 2063–2071.

[23] X. Q. Wang, Q. Q. Li, Y. Zhang, Y. F. Yang, S. X. Xiong, *Appl. Surf. Sci.* **2018**, *442*, 565–574.

[24] Y. Li, C. Chen, *J. Mater. Sci.* **2017**, *52*, 12348–12357.

[25] M. Thommes, K. Kaneko, A. V. Neimark, J. P. Olivier, F. Rodriguez-Reinoso, J. Rouquerol, K. S. W. Sing, *Pure Appl. Chem.* **2015**, *87*, 1051–1069.

[26] S. H. He, Z. P. Li, J. Q. Wang, P. Wen, J. C. Gao, L. M. Ma, Z. G. Yang, S. R. Yang, *RSC Adv.* **2016**, *6*, 49478–49486.

Q. Li, X. Wang,* N. Yang, F. He, Y. Yang, B. Wu, J. Chu,
A. Zhou, S. Xiong* **1–10**

Hydrangea-like NiCo-based Bimetal-organic Frameworks, and their Pros and Cons as Supercapacitor Electrode Materials in Aqueous Electrolytes